Spatial and temporal structure in systems of coupled nonlinear oscillators

Irene Waller and Raymond Kapral
Department of Chemistry, University of Toronto, Toronto, Ontario, Canada M5S 1A1
(Received 4 June 1984)

The spatial and temporal bifurcations of a ring of coupled, discrete-time, nonlinear oscillators are studied. The model displays many of the phenomena observed in diffusively coupled, nonlinear, chemical oscillators which can possess complex dynamics when isolated. The low-order bifurcation diagram of the discrete-time model may be computed analytically and shows how in-phase and out-of-phase solutions arise and undergo further bifurcations to quasiperiodic or chaotic states. Spatial bifurcations (pattern formation) accompany the temporal bifurcations and the results indicate how some of these processes occur. The phase diagram possesses self-similar scaling features associated with the higher-order periodic states. The model should prove useful in identifying the analogous phenomena in physical systems.

I. INTRODUCTION

Spatial and temporal pattern formation is commonly found in nature, most obviously in biological systems where coupling among autonomous oscillators can lead to self-organizing structures and rhythms, but examples also abound in other fields. Turing's well-known study[1] on the chemical basis of morphogenesis showed how symmetry-breaking bifurcations in reaction-diffusion equations may lead to spatial organization and a rather extensive literature now exists on the study of nonlinear reaction-diffusion systems.[2,3] Nonlinear chemical oscillators can exist in a wide variety of temporal states[4] even when "well stirred" so that diffusion plays no role: In addition to complex periodic solutions, chaotic states have also been observed and a number of specific routes to chaos have been identified.[5]

While spatial structure development in reaction-diffusion systems is typically described by partial differential equations, the same phenomena are exhibited by coupled arrays of well-stirred oscillators. Such systems have been studied experimentally and may be modeled by sets of ordinary differential equations. The interplay between spatial and temporal bifurcations may be more easily studied for these cellular models since the bifurcation parameters which specify the temporal states of the individual homogeneous oscillators and the coupling among the oscillators may be controlled. A number of studies of this type have revealed interesting phenomena, for instance, simple and complex synchronizations among the oscillators,[6] period doubling and quasiperiodicity even when the individual oscillators are only capable of limit-cycle behavior,[7] and multistability among diverse attracting states.[8]

We investigate such phenomena through the study of an even simpler model: an array of coupled discrete-time oscillators. More specifically our model consists of a ring of identical quadratic maps with general form $x_{t+1}=\lambda x_t(1-x_t)$, each oscillator being linearly coupled to its nearest neighbors. As λ varies, the map develops a complicated but structured temporal behavior.[9] Hence, by varying λ and the coupling parameter we may study how sets of coupled, complex, nonlinear oscillators behave. Even two such coupled oscillators have a rich bifurcation diagram.[10–12]

The model studied here may be considered to be a one-dimensional cellular automaton with an infinite number of possible states.[13] Much simpler two-state cellular automata display complex behavior, and multistate, two-dimensional automata have been used to model pattern formation in the Belousov-Zhabotinsky reaction.[14] While the model differs in a number of fundamental ways from coupled, continuous-time oscillators (these will be discussed below), it does exhibit many of the phenomena observed in real systems.

The model is described in detail in Sec. II and its low-order bifurcation structure is computed analytically. The results show how a number of spatial and temporal bifurcations occur in coupled oscillator systems displaced far from equilibrium and the nature of the multistability among different spatio-temporal states of the system. Calculations of the higher-order subharmonic bifurcations are also presented and the self-similar scaling nature of the phase diagram is discussed. The higher-order periodic, quasiperiodic, and chaotic states are studied in Sec. III. Such states may also exhibit spatial patterns and their character and structure in various regions of the bifurcation parameter plane are investigated. The results are discussed further in Sec. IV.

II. RINGS OF COUPLED MAPS

Consider a set of N, identical, nearest-neighbor-coupled, quadratic maps with periodic boundary conditions: a ring of quadratic maps. The discrete-time evolution of this system is governed by the equation

$$x(m,t+1)=\lambda x(m,t)[1-x(m,t)] +\gamma[x(m+1,t)-2x(m,t)+x(m-1,t)] , \tag{2.1}$$

 ©1984 The American Physical Society

where the index $m \in \{1, \ldots, N\}$ specifies the position on the ring and $x(1,t)=x(N+1,t)$ as a consequence of the periodic boundary condition. Letting $\vec{x}$ denote an N-dimensional vector, the map may be written compactly as $\vec{x}(t+1)=\vec{F}(\vec{x}(t);\lambda,\gamma)$, where $\vec{F}$ is a vector-valued function defined by the right-hand side (rhs) of Eq. (2.1).

As λ varies on [0,4],[15] an isolated quadratic map undergoes a complex sequence of bifurcations, which have been well documented.[9,16] The form of the coupling, whose strength is gauged by γ, clearly mimics that of diffusively coupled continuous-time oscillators, but the analogy is not perfect.[17]

Translational symmetry on the ring can be used to characterize the solutions: Attractors must possess the symmetry of the ring or exist in sets which have this symmetry; the dimension of such sets is a function of N and the bifurcation parameters. Complex multistability is also possible.

The analysis of the bifurcation structure of the ring of maps is conveniently carried out by Fourier transforming with respect to the position on the ring. (The analysis is similar to Turing's.) We define the Fourier transform as

$$\xi_j(t)=\frac{1}{N}\sum_{m=1}^{N} e^{-2\pi imj/N}x(m,t) \tag{2.2}$$

and Eq. (2.1) takes the form

$$\xi_j(t+1)=[\lambda-4\gamma\sin^2(\pi j/N)]\xi_j(t)-\lambda\sum_{k=0}^{N-1}\xi_k(t)\xi_{j-k}(t)\ . \tag{2.3}$$

The mode-coupling term arises from the nonlinear character of the oscillator.

A. Period-1 bifurcations

Two of the period-1 fixed points of the coupled-map system, $\vec{x}^*=\vec{F}(\vec{x}^*;\lambda,\gamma)$, are identical to those of an isolated map since the coupling term vanishes for such states. These fixed points are $x^*(m)=x^*=0$ and $x^*(m)=x^*=1-1/\lambda$ and their stability may be determined from the analysis of the linearized forms of Eqs. (2.1) or (2.3). (The other possible period-1 fixed points are unstable and will not be considered further.) Letting $x(m,t)=x^*+\delta x(m,t)$ and $\delta\xi_j(t)$ be the transform $\delta x(m,t)$, we obtain

$$\delta\xi_j(t)=[\eta^*-4\gamma\sin^2(\pi j/N)]^t\delta\xi_j(0)\ , \tag{2.4}$$

where $\eta^*=\lambda(1-2x^*)$. The condition for marginal stability of a particular Fourier component is

$$\eta^*-4\gamma\sin^2(\pi j/N)=\pm 1,\quad j=0,\ldots,N-1\ . \tag{2.5}$$

For the fixed point at the origin, $\eta^*=\lambda$ and the bifurcation boundaries may be determined from

$$0_j^{\pm}:\ \lambda=\pm 1+4\gamma\sin^2(\pi j/N)\ , \tag{2.6}$$

while for the fixed point at $x^*=1-1/\lambda$ we have $\eta^*=2-\lambda$ and

$$1_j^{\pm}:\ \lambda=(2\mp 1)-4\gamma\sin^2(\pi j/N)\ . \tag{2.7}$$

These equations specify a family of lines in the (λ,γ) plane that depend on the values of j and N.

The bifurcation boundaries of the period-1 fixed points are determined by the $0_j^{\pm}$ or $1_j^{\pm}$ lines first crossed, corresponding to marginal stability of a particular wavelength mode on the ring, all remaining modes being stable. The wavelength of a mode with index j is N/j. In the present case the boundaries are determined by modes with two wavelengths. In-phase-type bifurcations are determined by the extreme long-wavelength mode with $j=0$. For the $x^*=0$ fixed point this type of instability occurs at the γ-independent boundaries $\lambda=\pm 1$, while for $x^*=1-1/\lambda$ the boundaries are $\lambda=1,3$. These values of λ are identical to the bifurcation points of an isolated map since the coupling term vanishes for all in-phase solutions.

The remaining period-1 boundaries are determined by the extreme short-wavelength modes. Here we must distinguish between even and odd values of N. For N even[18] the marginally stable mode is $j=N/2$ and the boundaries are $\lambda=\pm 1+4\gamma$ for $x^*=0$ and $\lambda=(2\mp 1)-4\gamma$ for $x^*=1-1/\lambda$. This mode, with wavelength equal to 2, corresponds to a strictly alternating pattern on the ring, every other oscillator being equivalent. These boundaries (along with others to be discussed subsequently) are shown in Fig. 1. Thus, for N even the period-1 boundaries are independent of N. On the other hand, when N is odd the relevant modes have $j=(N\pm 1)/2$ yielding the boundary equations

$$\lambda=\pm 1+4\gamma\sin^2[(N\pm 1)\pi/2N]\quad \text{for } x^*=0$$

$$\lambda=(2\mp 1)-4\gamma\sin^2[(N\pm 1)\pi/2N]\quad \text{for } x^*=1-1/\lambda$$

which now clearly depend on N since the strictly alternating mode is not compatible with the odd number of oscillators on the ring. There are $(N+1)/2$ inequivalent oscillators for odd N. Of course, as $N\to\infty$, the odd-N boundaries approach those for even N (see Fig. 1).

The above analysis provides the boundaries of the two parallelogram-shaped regions in Fig. 1 within which the two period-1 fixed points are stable. We next consider the nature of the subsequent bifurcations in this system. The analysis will only be carried out for the even-N case al-

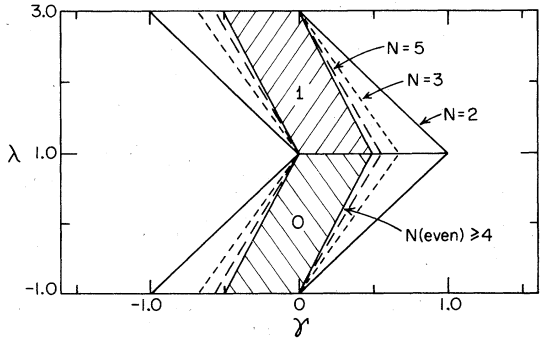

FIG. 1. Period-1 boundaries: the lower region, labeled 0, refers to the fixed point at the origin, $x^*(m)=0$, while 1 refers to the nontrivial fixed point $x^*(m)=1-1/\lambda$. The region of stability for N(even) ≥ 4 is scored.

though we shall discuss some features of the odd-N results. The fixed point $x^*=1-1/\lambda$ is unstable for $\lambda>3$ and, as discussed above, the instability occurs through the $j=0$ infinite-wavelength mode. This corresponds to bifurcation to an in-phase period-2 orbit. The region of stability of this orbit may be studied by a simple extension of the previously given analysis.

B. In-phase, period-2 bifurcations

The in-phase, period-2 fixed points are identical to those of an isolated map:

$$\left.\begin{aligned} x_1^*(m)&=x_1^* \\ x_2^*(m)&=x_2^* \end{aligned}\right\}=(2\lambda)^{-1}\{\lambda+1\pm[(\lambda-3)(\lambda+1)]^{1/2}\}\ ; \quad (2.8)$$

every oscillator on the ring is identical to its neighbor, the fixed-point values alternating between x_1^* and x_2^* on successive iterates of the map. Since each oscillator is independent of its neighbor, the system behaves like N independent period-2 oscillators set in phase to "fire" synchronously. While the nature of this state is independent of the coupling γ, its stability does depend on γ as for the period-1 states. The stability of the state may be investigated by considering the second power of Eq. (2.1), $\vec{x}(t+2)=\vec{F}(\vec{F}(t))$, linearized about the in-phase, period-2 fixed points. Letting $x(m,t)=x_{1,2}^*+\delta x(m,t)$ we have

$$\delta x(m,t+2)=A\,\delta x(m,t)+B[\delta x(m+1,t)+\delta x(m-1,t)] +\gamma^2[\delta x(m+2,t)+\delta x(m-2,t)]\ , \quad (2.9)$$

with

$$A=\lambda^2(1-2x_1^*)(1-2x_2^*)-4\lambda\gamma(1-x_1^*-x_2^*)+6\gamma^2 \quad (2.10)$$

and

$$B=2\lambda\gamma(1-x_1^*-x_2^*)-4\gamma^2\ . \quad (2.11)$$

Fourier transformation of Eq. (2.9) yields the time evolution of the ring collective modes for every other iterate of the map:

$$\delta\xi_j(2t)=[A+2B\cos(2\pi j/N)+2\gamma^2\cos(4\pi j/N)]^{2t}\delta\xi_j(0)\ . \quad (2.12)$$

Again lines in the (λ,γ) plane may be calculated from the condition of marginal stability of modes with index j. We obtain

$$-\lambda^2+2\lambda+4+8\gamma\sin^2(\pi j/N)[2\gamma\sin^2(\pi j/N)+1]=\pm1\ , \quad (2.13)$$

where the explicit fixed-point values have been used in the prefactor of $\delta\xi(0)$. The lines corresponding to ±1 are

$$2_j^-(I):\ \lambda=1+\{6+8\gamma\sin^2(\pi j/N)[2\gamma\sin^2(\pi j/N)+1]\}^{1/2} \quad (2.14)$$

and

$$2_j^+(I):\ \lambda=1+\{4+8\gamma\sin^2(\pi j/N) \times[2\gamma\sin^2(\pi j/N)+1]\}^{1/2}\ . \quad (2.15)$$

These j-dependent lines are shown in Fig. 2 for $N=4$ and in Fig. 3 for $N=6$. The region of stable in-phase period-2 is labeled and its boundaries are indicated as heavy solid lines while the extensions of these lines outside the boundary region are dashed.

The $2_j^-(I)$ lines determine the subharmonic bifurcation boundaries to period-4 orbits, both in phase and out of phase. The $2_0^-(I)$ line is simply $\lambda=1+\sqrt{6}$ and since it corresponds to marginal stability of the infinite-wavelength mode, it signals bifurcation to an in-phase, period-4 orbit. While $2_0^-(I)$ determines the bifurcation to period-4 for positive γ, for $\gamma<0$ the family of lines $2_j^-(I)(j>0)$ yield bifurcation boundaries for out-of-phase, period-4 orbits, boundaries with decreasing j values determining the bifurcation process for larger negative values of γ (see Figs. 2 and 3). The spatial patterns corresponding to the different marginally stable modes for $N=4$ are shown in Fig. 4. When $\gamma\lesssim0$ the $j=N/2$ mode with wavelength equal to 2 governs the bifurcation process; this gives rise to a period-4 orbit with a strictly alternating spatial pattern (Fig. 4). For somewhat more negative values of γ the $2_{1,3}^-(I)$ curves form the bifurcation boundaries. The wavelength of the mode is 4 and several types of patterns are possible; these are shown in Fig. 4. In pattern (a) alternate oscillators on the ring have periods of 4

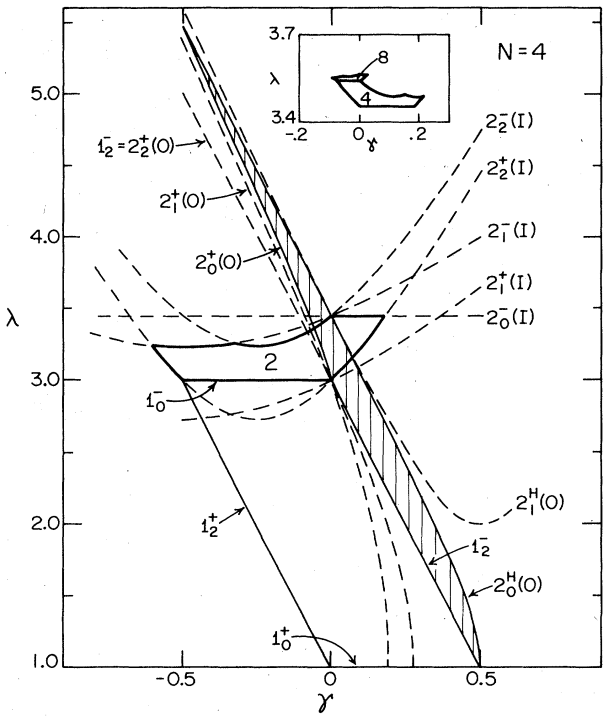

FIG. 2. Phase diagram for $N=4$ showing the period-1, -2, and -4 states. The notation for the various lines is discussed in the text. The region 2 denotes in-phase, period 2 while the scored region denotes out-of-phase, period 2. The in-phase, period-4, and period-8 regions are shown in the inset with the vertical scale magnified by two in order to make their structure clearer; each in-phase 2^{n+1} region is a scaled-down mirror image of the 2^n region below it.

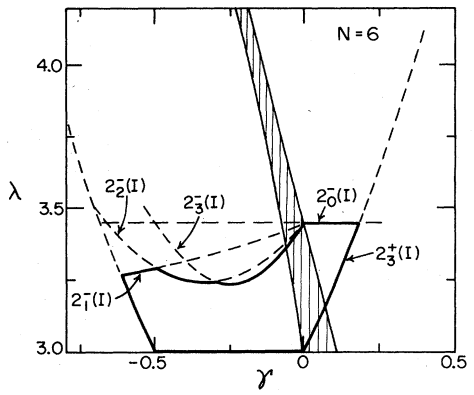

FIG. 3. Detail of the in-phase, period-2 region for $N=6$ showing the sequence of $2_j^-(I)$ lines determining the bifurcation boundary to a number of different types of out-of-phase, period-4 orbits. The out-of-phase, period-2 region is scored.

and 2, respectively. This is a rhythm-splitting pattern. In (b) there are two pairs of equivalent oscillators with an overall temporal period of 4, while in (c) all four oscillators are inequivalent. Similar but more elaborate spatial patterns are possible for larger N. Each such attractor has its own basin, and multistability is possible.

Subharmonic bifurcation of an in-phase, period-2 orbit to in-phase or out-of-phase period-4 orbits occurs when the $2_j^-(I)$ boundaries are crossed. This in-phase, period-2 region can be closed by considering the $2_j^+(I)$ boundaries,

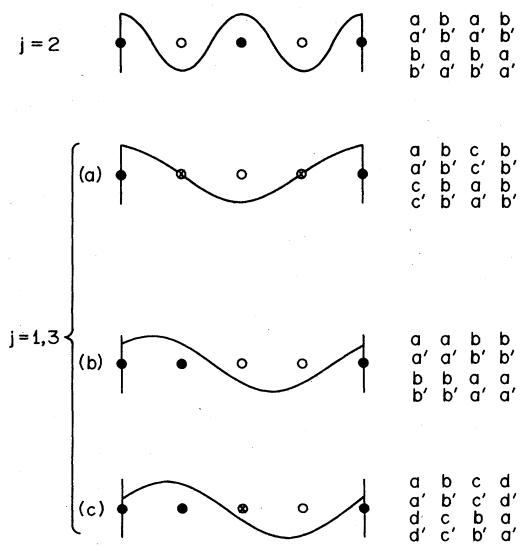

FIG. 4. Spatial patterns corresponding to the marginally stable collective modes for the $2_j^-(I)$ boundaries for $N=4$. The $j=2$ mode leads to a period-4 state with strictly alternating pattern. There are three possible states for $j=1,3$: (a) a rhythm-splitting pattern where two period-4 oscillators are separated by period-2 oscillators; (b) two pairs of equivalent period-4 oscillators; (c) four inequivalent period-4 oscillators. The fixed-point pattern corresponding to each of these states is shown on the right-hand side of the diagram.

which are the analogs of the tangent boundaries in one-dimensional maps. The $j=N/2$ mode determines this boundary: to the left of the boundary escape occurs, while to the right the in-phase, period-2 orbit loses its stability but other finite attractors exist in this region.

It is not difficult to generalize this procedure to calculate the boundaries for the in-phase orbits with arbitrary period n. We may write the equation for $\xi_j(t+1)$ compactly as $\vec{\xi}(t+1)=\vec{\mathbf{H}}(\vec{\xi}(t);\lambda,\gamma)$, where the vector-valued, nonlinear function $\vec{\mathbf{H}}$ is defined by the rhs of Eq. (2.3). The linearized form of the nth power of this equation may be used to determine the stability of the period-n orbits:

$$\delta\vec{\xi}(t+n)=\left[\frac{\partial\vec{\mathbf{H}}^{(n)}}{\partial\vec{\xi}}\right]_{\vec{\xi}=(\vec{\xi}^{(i)})^*}\cdot\delta\vec{\xi}(t),\quad i=1,\ldots,n\ . \tag{2.16}$$

The derivative matrix can be written in the alternate form

$$\left[\frac{\partial\vec{\mathbf{H}}^{(n)}}{\partial\vec{\xi}}\right]_{\vec{\xi}=(\vec{\xi}^{(i)})^*}=\underline{H}'((\vec{\xi}^{(1)})^*)\underline{H}'((\vec{\xi}^{(2)})^*)\times\cdots\underline{H}'((\vec{\xi}^{(n)})^*)\ , \tag{2.17}$$

by using the chain rule. For the in-phase orbits we have the further simplification that $(\xi_j^{(i)})^*=x_i^*\delta_{j0}$, $i=1,\ldots,n$, where x_i^* is one of the n fixed points of a single, isolated, quadratic map. Defining $\omega^{(i)}(j)$ as

$$\omega^{(i)}(j)=\lambda(1-2x_i^*)-4\gamma\sin^2(\pi j/N)\ , \tag{2.18}$$

we have

$$\left[\frac{\partial\vec{\mathbf{H}}^{(n)}}{\partial\vec{\xi}}\right]_{\vec{\xi}=(\vec{\xi}^{(i)})^*}=\prod_{i=1}^{n}\omega^{(i)}(j)\mathbb{1}\ . \tag{2.19}$$

The boundaries for the period-n orbits may then be determined from the solutions of the equations corresponding to marginal stability:

$$\prod_{i=1}^{n}\omega^{(i)}(j)=\pm1\ . \tag{2.20}$$

Since the fixed points are independent of γ, Eq. (2.20) may be easily solved for any fixed j and N. As an example, the period-4 and period-8 boundaries for $N=4$ are shown in Fig. 2. It is evident that the in-phase, period-4 region is a scaled down, mirror image of the in-phase, period-2 region; the in-phase regions corresponding to higher-order subharmonics scale in a similar way producing a phase diagram with self-similar scaling features. In fact, it is not difficult to deduce the scaling properties of these regions. The maximum heights of the in-phase regions clearly have the same λ scaling as the isolated quadratic maps, i.e., they scale as Feigenbaum's $\delta=4.669\ldots$. The width scaling follows simply from Eq. (2.20) and may be shown to be $\gamma\sim\alpha^{-n}$, where α is Feigenbaum's orbit scaling exponent, $\alpha=2.5029\ldots$. Thus, the heights of the the regions contract more rapidly than the widths giving rise to very flat regions for large n.

The in-phase, period-2 orbit whose bifurcation structure

was discussed in this section was born out of the period-1 state via the instability of the extreme long-wavelength mode $j=0$; this orbit may also bifurcate through marginal stability of the extreme short-wavelength mode $j=N/2$ giving rise to an out-of-phase, period-2 orbit. In Sec. II C we explore the stability of this out-of-phase state.

C. Out-of-phase, period-2 bifurcations

When N is even the period-2 orbit that results from the bifurcation of the period-1 fixed point $x^*(m)=1-1/\lambda$ has a strictly alternating pattern on the ring. The region of stability in the (λ,γ) plane of this orbit may be determined by a procedure similar to that described above; now, however, one must linearize the second-power map equations about each of the separate fixed points, which alternate around the ring.[19] If we denote these fixed points by $x^*(m)=x_1^*$ for $m=2k$ and $x^*(m)=x_2^*$ for $m=2k+1$, linearization of the second-power map leads to

$$\begin{aligned}\delta x(2k,t+2) &= \mathscr{A}\delta x(2k,t)+\mathscr{B}[\delta x(2k+1,t)+\delta x(2k-1,t)] \\ &\quad +\gamma^2[\delta x(2k+2,t)+\delta x(2k-2,t)] , \end{aligned} \tag{2.21}$$

where $\mathscr{A}=A$ defined in Eq. (2.10) but the fixed points x_1^* and x_2^* are now those for the out-of-phase, period-2 orbit[18]

$$\left.\begin{matrix}x_1^* \\ x_2^*\end{matrix}\right\} = \tfrac{1}{2}+\lambda^{-1}(\tfrac{1}{2}-2\gamma)\pm\lambda^{-1}[\,\lambda(\tfrac{1}{4}\lambda-\tfrac{1}{2})-(1-2\gamma)^2 +\tfrac{1}{4}]^{1/2} . \tag{2.22}$$

The coefficient $\mathscr{B}$ is defined by

$$\mathscr{B}=2\lambda\gamma(1-2x_2^*)-4\gamma^2 . \tag{2.23}$$

A similar expression may be written for the relaxation of perturbations at odd positions on the ring; the equation takes the same form with $2k$ replaced by $2k+1$ and $\mathscr{B}$ replaced by $\tilde{\mathscr{B}}$, which can be obtained from Eq. (2.23) by replacing x_2^* by x_1^*. These equations may be solved by introducing the following transformations:

$$\delta\xi_j^{(e)}(t)=\frac{2}{N}\sum_{k=1}^{N/2} e^{-2\pi i 2jk/N}\delta x(2k,t) \tag{2.24}$$

and

$$\delta\xi_j^{(0)}(t)=\frac{2}{N}\sum_{k=0}^{N/2-1} e^{-2\pi ij(2k+1)/N}\delta x(2k+1,t) . \tag{2.25}$$

Under these transformations Eq. (2.21) and its mate reduce to the matrix equation

$$\begin{bmatrix}\delta\xi_j^{(e)}(t+2)\\ \delta\xi_j^{(0)}(t+2)\end{bmatrix}=\underline{M}(j)\begin{bmatrix}\delta\xi_j^{(e)}(t)\\ \delta\xi_j^{(0)}(t)\end{bmatrix} , \tag{2.26}$$

with

$$M_{11}(j)=M_{22}(j)=\mathscr{A}+2\gamma^2\cos(4\pi j/N)$$

and

$$M_{12}(j)=2\mathscr{B}\cos(2\pi j/N) , \quad M_{21}(j)=2\tilde{\mathscr{B}}\cos(2\pi j/N) . \tag{2.27}$$

The problem is now formally similar to the two-morphogen case treated by Turing.[1] Since a 2×2 problem must be solved for each j, there is a correspondingly richer solution structure. Equation (2.26) may be solved for the even and odd perturbations by diagonalizing $\underline{M}$; we find

$$\delta\xi_j^{(e)}(2t)=\tfrac{1}{2}[\,(\epsilon_1^{2t}+\epsilon_2^{2t})\delta\xi_j^{(e)}(0) +(\mathscr{B}/\tilde{\mathscr{B}})^{1/2}(\epsilon_1^{2t}-\epsilon_2^{2t})\delta\xi_j^{(0)}(0)] \tag{2.28}$$

and

$$\delta\xi_j^{(0)}(2t)=\tfrac{1}{2}[\,(\mathscr{B}/\tilde{\mathscr{B}})^{1/2}(\epsilon_1^{2t}-\epsilon_2^{2t})\delta\xi_j^{(e)}(0) +(\epsilon_1^{2t}+\epsilon_2^{2t})\delta\xi_j^{(0)}(0)] . \tag{2.29}$$

The eigenvalues $\epsilon_{1,2}$ of $\underline{M}$ are

$$\epsilon_{1,2}(j)=\mathscr{C}+4\gamma^2[1+\cos^2(2\pi j/N)] \pm4\gamma(\mathscr{C}+4\gamma^2)^{1/2}\cos(2\pi j/N) , \tag{2.30}$$

with

$$\mathscr{C}=-\lambda^2+2\lambda+4+4\gamma(4\gamma-5) . \tag{2.31}$$

When studying the solution structure we may distinguish two cases: real eigenvalues and complex eigenvalues.

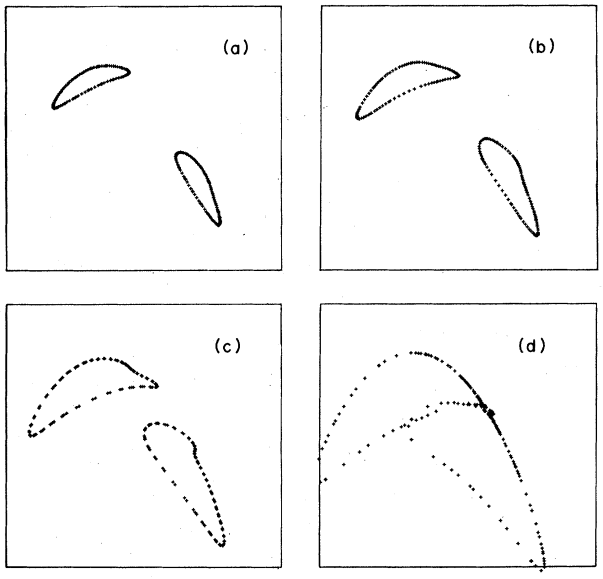

FIG. 5. Projections of the dynamics for $N=4$ on the $[x(1,t),x(1,t+1)]$ plane. Projections on the other oscillator coordinates have identical forms. The figures correspond to $\lambda=2.5$ and an increasing sequence of γ values. The maximum Lyapanov exponents 1_{max} were computed to determine if the state was quasiperiodic or chaotic: (a) $\gamma=0.25$, $1_{max}=-0.0002$, quasiperiodic; (b) $\gamma=0.26$, $1_{max}=0.0003$, quasiperiodic; (c) $\gamma=0.27$, $1_{max}=0.0005$, quasiperiodic; (d) $\gamma=0.29$, $1_{max}=0.175$, chaotic.

If the eigenvalues are complex and the complex-conjugate pair passes through the unit circle, the system undergoes a Hopf bifurcation. Using Eq. (2.30) the condition for such a bifurcation may be written as

$$[\mathscr{C}+4\gamma^2\sin^2(2\pi j/N)]^2=1\ , \tag{2.32}$$

which yields the Hopf lines in the (λ,γ) plane

$$2_j^H(0):\ \lambda=1+[6+4\gamma(4\gamma-5)+4\gamma^2\sin^2(2\pi j/N)]^{1/2}\ . \tag{2.33}$$

These lines are sketched in Fig. 2 for $N=4$ (and partially for $N=6$ in Fig. 3). The $j=0$ and $j=N/2$ modes determine the boundaries for this bifurcation. Since the transforms are carried out on alternate oscillators on the ring, both j values correspond to extreme long-wavelength modes on the ring. The relaxation is now oscillatory about each type of fixed point suggesting bifurcation to N invariant circles with the symmetry of the out-of-phase period-2 state. This is indeed found in the numerical simulations and results for $N=4$ are shown in Fig. 5. The other $2_j^H(0)$ lines lie to the right of $2_j^H(0)=2_{N/2}^H(0)$ and do not determine the bifurcation boundaries for any (even) N. Note, however, that the lines touch at $(\lambda=1+\sqrt{6},\gamma=0)$.

The other type of bifurcation of an out-of-phase period-2 orbit occurs when the eigenvalues of $\underline{M}$ are real. The marginal case now occurs when one eigenvalue, say, ϵ_1, satisfies $|\epsilon_1|=1$ while $|\epsilon_2|<1$. In fact for real eigenvalues we must have $\epsilon_1=+1$ and the bifurcation is analogous to a tangent bifurcation in the one-dimensional case. The lines corresponding to this marginal case are given by

$$2_j^+(0):\ \lambda=1+2\{1+2\gamma(2\gamma-3)+2\gamma\sin^2(\pi j/N)[1+2\gamma-2\gamma\sin^2(\pi j/N)]\}^{1/2}\ . \tag{2.34}$$

The equivalent $j=0$ and $j=N/2$ modes again determine the boundaries for this bifurcation; this boundary along with the other $2_j^+(0)$ lines are shown in Fig. 2 for $N=4$ where the region in the (λ,γ) plane corresponding to stable out-of-phase, period-2 orbits is scored with heavy lines. The $2_0^H(0)$ and $2_0^+(0)$ boundaries cross at $(\lambda=1+2\sqrt{5},\gamma=-\frac{1}{2})$.

Hence, for N even the low-order bifurcation structure may be computed analytically for rings of quadratic maps. The $0_{0,N/2}^{\pm}$, $1_{0,N/2}^{\pm}$, $2_{0,N/2}^{+}(I)$, $2_0^H(0)=2_{N/2}^H(0)$, and $2_0^+(0)=2_{N/2}^+(0)$ boundaries are *independent of* N (for N even), while the $2_j^-(I)$ boundaries change as N varies leading to the spatially different patterns for out-of-phase, period-4 orbits. As a consequence most of the structure displayed in Fig. 2 is true for any even N.[18] The boundaries for odd N are more difficult to compute because the symmetry of the system is lower after the first symmetry-breaking bifurcation. Since the out-of-phase, period-2 state is not strictly alternating, one must in general solve higher-order sets of coupled equations for the boundary lines. For large N one expects that the odd-N boundaries will approach those given above as was the case for the $0^{\pm}$ and $1^{\pm}$ boundaries.

III. QUASIPERIODIC AND CHAOTIC STATES

Complex behavior is observed in regions of the parameter plane outside those corresponding to the low-order periodic states discussed in the preceding section. In fact, these coupled oscillator systems display all of the routes to chaos mentioned in the Introduction but now accompanied or interrupted by spatial bifurcations.

Along the line $\gamma=0$ the system is, of course, like N isolated quadratic maps and exhibits period-doubling cascades as well as intermittency transitions into chaos; these mechanisms also operate for $\gamma\neq0$ for the in-phase orbits. We noted that period doubling from the out-of-phase, period-2 orbit does not occur. Instead the system undergoes a Hopf bifurcation and quasiperiodicity ensues; projections of the quasiperiodic attractor (in N-dimensional space) onto the $[x(m,t+1),x(m,t)]$ plane are a set of $2N$ invariant circles. As λ and γ are tuned these circles distort and break up leading to chaotic behavior. This breakup process is accompanied by sequences of mode lockings which give rise to stable periodic orbits. For circle maps (and for two-coupled oscillators) this mechanism for the onset of chaos is being actively studied and many aspects of the scaling theory of such phenomena are now understood.[20–23] For N coupled maps the various spatial bifurcations that occur during this process must also be taken into account. By way of illustration we now consider some of these processes, first for even N and then for $N=3$ as an example of the attractor structure for odd N.

Since the $j=0$ $(N/2)$ mode in our alternate site Fourier representation determines the Hopf boundary, the invariant circles for even N have strictly alternating symmetry about the ring with regard to their phase relations, but their projections onto the $[x(m,t+1),x(m,t)]$ planes are identical. A sequence of such projections for $N=4$ and $\lambda=2.5$ with increasing γ is shown in Fig. 5. Throughout this progression the temporal behavior of the attractor maintains an alternating phase relationship around the ring, each oscillator projection having the same appearance as its neighbors. (Consequently only one such projection is shown for each set of parameter values.) Thus, the spatial symmetry is preserved through a range of temporal periodic, quasiperiodic, and chaotic states. (The character of the state was determined from the value of the maximum Lyapunov exponent,[24] $l_{\max}$; $l_{\max}<0$ for periodic states, $l_{\max}=0$ for quasiperiodic states, and $l_{\max}>0$ for chaotic states.)

For greater (even) N values the strictly alternating phase relationship is not maintained over as wide a range of γ values but bifurcation is always to a quasiperiodic state with this symmetry; as N increases the region corresponding to the strictly alternating state shrinks and other spatial bifurcations intervene. The results for a ring of six oscillators shown in Figs. 6(a)–6(d) illustrate the types of bifurcation pattern which can occur for larger N values. In all figures the dynamics of each oscillator is again

represented by its projection on the $[x(m,t+1),x(m,t)]$ plane. Figure 6(a) displays the quasiperiodic attractor which exists near the out-of-phase, period-2 boundary; while each projection appears identical to that of its neighbor, again the time series of alternate oscillator coordinates are identical. As γ increases, the circles distort and break up as in the $N=4$ case but now these bifurcations are accompanied by states with new spatial symmetry. Spatial bifurcations may occur as the coupling parameter is tuned as shown in Fig. 6(b). Here the quasiperiodic attractor possesses the spatial symmetry (1)=(2), (3)=(6), and (4)=(5) [oscillator positions on the ring will be denoted by (m)] but the time series of the oscillator coordinates are different. In Fig. 6(c) the projections of the chaotic attractor display rough spatial symmetry of the form (1)=(6), (2)=(5), and (3)=(4), while again the time series of all oscillator coordinates are different from each other. In the final figure [6(d)] a chaotic state exists which looks like six very noisy quadratic maps in our projection. Beyond this chaotic state the system mode locks on a period-2 state with the following symmetry: (1)=(4), and (2)=(3)=(5)=(6). The results described above are not particular for the chosen examples; we have observed similar phenomena for larger N. Because of the various possible symmetry-related states for large N one must also deal with multistability of the different attractors and the dispositions of their associated basins. We have not attempted to give a systematic classification of these higher-order spatial and temporal bifurcations or an enumeration of possible coexisting states.

The bifurcations to invariant circles occur from many of the out-of-phase states. For instance, the out-of-phase, period-4 orbits described earlier bifurcate in this way as is shown in Fig. 7. As the bifurcation parameter λ is tuned, a subharmonic cascade of in-phase periodic solutions exists for positive γ near zero; correspondingly for negative γ each of these orbits may bifurcate to out-of-phase orbits with doubled period that in turn undergo Hopf bifurcation to a quasiperiodic state. A rich but highly structured solution hierarchy exists which exhibits scaling features.

Since the quasiperiodic and chaotic attractors reside in an N-dimensional space their structure is not completely revealed by the representations adopted thus far. In order to examine the nature of some of these states in more detail we consider the three-oscillator case for which simple graphical representations are still useful.

We saw that for odd N, bifurcation to the out-of-phase period-2 state occurs via marginal stability of the extreme short-wavelength mode with $j=(N\pm1)/2$ and leads to a period-2 orbit with $(N+1)/2$ equivalent oscillators. As anticipated, our numerical results indicate that Hopf bifurcation to the quasiperiodic state maintains this symmetry. For $N=3$ there is one distinct and a pair of identical oscillators on the ring and, thus, there are three such coexisting period-2 states corresponding to the three different possibilities for the distinct oscillator. This symmetry is preserved beyond the Hopf bifurcation giving rise to three pairs of invariant circles in the three-dimensional space, each with its own basin [see Fig. 8(a)]. This illustrates one of the complications for the odd-N case. Multistability of the attractors appears immediately after bifurcation from

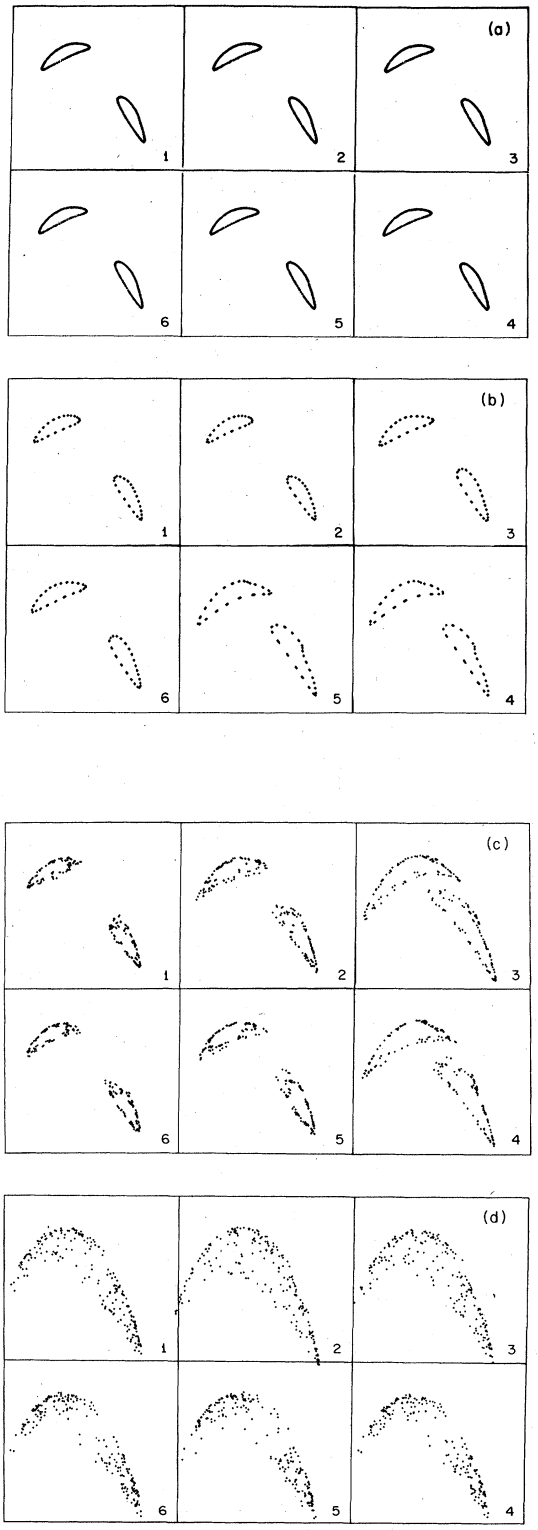

FIG. 6. Spatial and temporal bifurcation patterns for a ring of six oscillators. In all figures $\lambda=2.5$. (a) $\gamma=0.25$, strictly alternating temporal quasiperiodic state, identical spatial structure; (b) $\gamma=0.26$, quasiperiodic state with temporal structure; (c) $\gamma=0.27$, chaotic temporal state with (rough) spatial structure; (d) $\gamma=0.27$, highly evolved chaotic state.

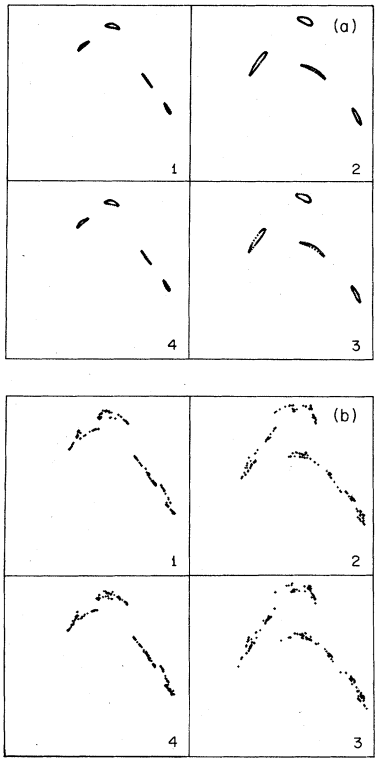

FIG. 7. Quasiperiodic and chaotic states arising from an out-of-phase, period-4 orbit. (a) $\lambda=3.4, \gamma=-0.25$, quasiperiodic state; (b) $\lambda=3.45, \gamma=-0.25$, chaotic state.

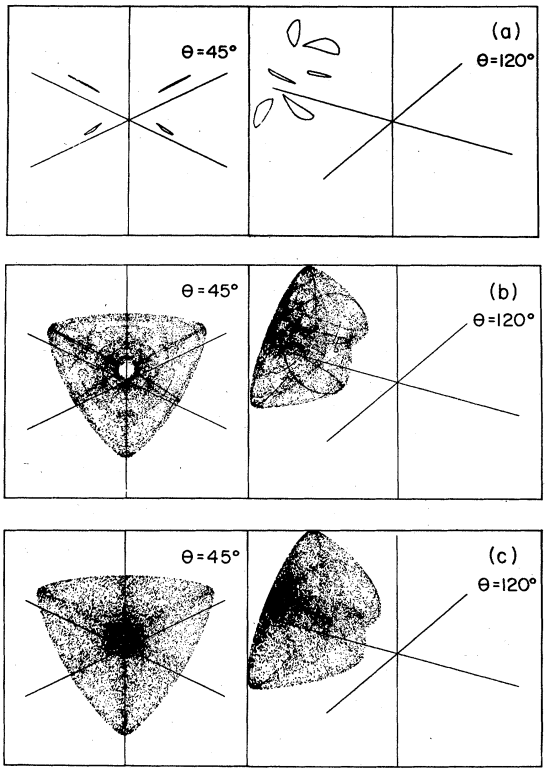

FIG. 8. Quasiperiodic and chaotic attractors for $N=3$. (a) Three quasiperiodic attractors for $\lambda=2.5$ and $\gamma=0.34$; $1_{max}=-0.0003$. (b) Chaotic attractor at $\lambda=2.5$ and $\gamma=0.38$; $1_{max}=0.10$. (c) Chaotic attractor at $\lambda=2.5$ and $\gamma=0.40$; $1_{max}=0.19$. Two projections are shown for each attractor: $\theta=45°$ and 120°.

the period-1 state. The invariant circles suffer the same fate as described earlier for the even-N case. They deform, undergo a sequence of mode lockings, and finally give rise to a chaotic attractor, which is shown in Fig. 8(b). This three-dimensional attractor has a rather interesting structure which contains remnants of the three pairs of circles which have broken up. In the chaotic state the three attracting regions are no longer distinct, although iterates are clearly concentrated in the neighborhood of the now unstable invariant circles. Iterates wander in a three-dimensional region of phase space but spend large amounts of time in the now broken circles. The attractor also possesses features which can be related to the stability analysis of the period-1 fixed point $x^*(m)=1-1/\lambda$, whose secondary bifurcations led to the chaotic state. The linearized stability analysis yields eigenvalues $\epsilon_1=2-\lambda$ and $\epsilon_{2,3}=2-\lambda-3\gamma$ characterizing the relaxation about this fixed point. For the parameter values of interest $|\epsilon_1|<1$ while $|\epsilon_{2,3}|>1$. The attractor possesses rotational symmetry about $\vec{u}_1=(3)^{-1/2}(1,1,1)$ the stable direction eigenvector corresponding to ϵ_1 and, in fact, has a hole from which iterates are excluded. As γ increases, the attractor expands and encompasses this stable manifold of the period-1 fixed point. When this happens the hole ceases to exist and iterates may access the unstable fixed point [Fig. 8(c)].

The above results for $N=3$ provide some indication of the kinds of quasiperiodic and chaotic attractors that systems of coupled dissipative oscillators could possess. In these higher-dimensional systems hyperchaotic attractors (more than one Lyapanov exponent is positive) may exist and give rise to complex aperiodic temporal behavior.

IV. DISCUSSION

The ring of quadratic maps was introduced as a model for a coupled set of nonlinear oscillators whose intrinsic (isolated) dynamics may be complex. The first few bifurcations in the discrete-time model can be studied analytically and the results show how in-phase and out-of-phase solutions arise and undergo further characteristic types of bifurcation: the in-phase solutions, which correspond to infinitely long-wavelength collective modes on the ring, may bifurcate to yield period-doubled, in-phase or out-of-phase solutions with different wavelengths; the out-of-phase solutions, on the other hand, cannot period double and instead undergo a Hopf bifurcation to a quasiperiodic state. Spatial structure accompanies the subsequent temporal bifurcations leading to quasiperiodic or even chaotic temporal states corresponding to specific collective modes on the ring. In addition, we saw that a number of different types of synchronization phenomena like those observed in coupled continuous-time nonlinear oscillators were found. Thus, the model may have utility for the analysis and prediction of the kinds of behavior that may

be observed in continuous-time systems, which are more difficult to analyze.

A number of features of the map model differ from those of coupled chemical oscillators with diffusive coupling. In the model, the coupling acts only at discrete time units. While map models are typically derived from flows through a Poincaré surface of section, it is not a simple matter to generalize this construction in a manner that obviously leads to the present map system. Furthermore, in continuous-time systems the full dynamical behavior of a limit-cycle oscillator may be followed and different types of synchronization behavior are possible. The full structure of phase resetting cannot be examined with a map model. Because of these differences the ring of maps should be regarded as an abstract model of coupled, complex, identical nonlinear oscillators that suggests some of the kinds of phenomena that may be observed in coupled oscillator systems in far-from-equilibrium states. In particular, the global structure of the higher-order bifurcations involving out-of-phase periodic, quasiperiodic, and chaotic states should be amenable to more detailed analysis, especially with regard to its scaling properties. Analogous phenomena should be observable in systems of coupled continuous-time oscillators, for instance in diffusively coupled cells of chemical oscillators. Some aspects of the analysis of these higher-order bifurcations are like Turing's treatment of the morphogenesis problem but with many morphogens. Since we are dealing with secondary bifurcations far from equilbrium we observe a much more elaborate spatial and temporal bifurcation structure than that observed through bifurcation of a simple steady state. The present work may serve as a guide to the kinds of bifurcations to be expected in these far-from-equilibrium states.

ACKNOWLEDGMENTS

This research was supported in part by a grant from the Natural Sciences and Engineering Research Council of Canada. We would also like to thank E. Celarier for his help in preparing the figures for publication.

[1]A. M. Turing, Philos. Trans. R. Soc. London, Ser. B **237**, 37 (1952).

[2]G. Nicolis and I. Prigogine, *Self-Organization in Nonequilibrium Systems* (Wiley, New York, 1977).

[3]A. Pacault and C. Vidal, J. Chim. Phys. **79**, 691 (1982).

[4]See, for instance, J.-C. Roux, Physica D **7**, 57 (1983); J.-C. Roux and H. L. Swinney, in *Nonlinear Phenomena in Chemical Dynamics,* edited by A. Pacault and C. Vidal (Springer, New York, 1981); R. A. Schmitz, R. K. Graziani, and J. L. Hudson, J. Chem. Phys. **67**, 3040 (1977); I. Epstein, J. Phys. Chem. **88**, 187 (1984).

[5]E. Ott, Rev. Mod. Phys. **53**, 655 (1981); J. P. Eckmann, *ibid.* **53**, 643 (1981).

[6]M. Marek and I. Stuchl, Biophy. Chem. **3**, 241 (1975); H. Fujii and Y. Sawada, J. Chem. Phys. **69**, 3830 (1978); K. Nakajima and Y. Sawada, *ibid.* **72**, 2231 (1980).

[7]I. Schreiber and M. Marek, Physica D **5**, 258 (1982); M. Sano and Y. Sawada, Phys. Lett. **97A**, 73 (1983); I. Schreiber and M. Marek, *ibid.* **91A**, 263 (1982); X.-J. Wang (unpublished).

[8]M. Kawato and R. Suzuki, J. Theor. Bio. **86**, 547 (1980); I. Stuchl and M. Marek, J. Chem. Phys. **77**, 2956 (1982).

[9]M. J. Feigenbaum, J. Stat. Phys. **19**, 25 (1978); **21**, 669 (1979); P. Collet and J.-P. Eckmann, *Iterated Maps on the Interval as Dynamical Systems* (Birkhauser, Boston, 1980).

[10]K. Kaneko, Prog. Theor. Phys. **69**, 1427 (1983).

[11]J.-M. Yuan, M. Tung, D. H. Feng, and L. M. Narducci, Phys. Rev. A **28**, 1662 (1983).

[12]T. Hogg and B. A. Huberman, Phys. Rev. A **29**, 275 (1984).

[13]For a discussion of cellular automata see, for instance, S. Wolfram, Rev. Mod. Phys. **55**, 601 (1983).

[14]W. Freedman and B. Madore, Science **222**, 615 (1983); J. M. Greenberg, B. D. Hassard, and S. P. Hastings, Bull. Am. Math. Soc. **84**, 1296 (1978).

[15]In the coupled system the relevant range of λ lies on a larger interval.

[16]R. M. May, Nature **261**, 459 (1976).

[17]While a one-dimensional quadratic map models many strongly dissipative flows, the coupled system Eq. (2.1) implies a further assumption about the nature of the discrete-time coupling among the oscillators.

[18]$N=2$ is a special case; its boundaries and fixed points may be obtained from the general even-N results by replacing γ by $\gamma/2$.

[19]A similar analysis may be carried out for the odd-N out-of-phase, period-2 states but it is technically more involved due to the fact that there are now $(N+1)/2$ inequivalent oscillators.

[20]D. Rand, S. Ostlund, J. Sethna, and E. Siggia, Phys. Rev. Lett. **49**, 132 (1982).

[21]M. J. Feigenbaum, L. P. Kadanoff, and S. J. Shenker, Physica (Utrecht) **50**, 370 (1982).

[22]K. Kaneko, Prog. Theor. Phys. **68**, 669 (1982).

[23]For a discussion of some of the scaling properties of such systems in regions where the invariant circles have broken, see M. Schell, S. Fraser, and R. Kapral, Phys. Rev. A **28**, 373 (1983); J. Belair and L. Glass, Phys. Lett. **96A**, 113 (1983); S. Fraser and R. Kapral, Phys. Rev. A **30**, 1017 (1984).

[24]G. Benettin, L. Galgani, A. Giorgilli, and J.-M. Strelcyn, Meccanica **15**, 21 (1980).